Electronic structure of InN studied using soft X-ray emission, soft X-ray absorption, and quasiparticle band structure calculations

L. F. J. Piper*, L. Colakerol, T. Learmonth, and K. E. Smith
Department of Physics, Boston University, Boston, MA 02215

F. Fuchs, J. Furthmüller and F. Bechstedt
Institut für Festkörpertheorie und -optik Friedrich-Schiller-Universität Jena Max-Wien-Platz 1 D-07743 Jena, Germany

Tai-Chou Chen, and T. D. Moustakas
Electrical and Computer Engineering Department, Boston University, Boston, MA 02215

J. -H. Guo
Advanced Light Source, Lawrence Berkeley National Laboratory, Berkeley, California 94720

The electronic structure of wurtzite InN($000\bar{1}$) thin films has been studied using a combination of soft x-ray emission and absorption spectroscopies. We measured the elementally and orbitally resolved InN valence and conduction bands by recording the N *K*-edge spectra. Theoretical calculations of the N 2*p* partial density of states were performed within the GW framework of many body perturbation theory. Good agreement between the experimental spectra and the calculations was obtained, most notably with the energetic location of the In 4*d* - N 2*p* hybridized state in the emission spectrum and the angular dependence of the absorption spectra.

PACS numbers: 71.20.Nr, 78.70.En, 78.70.Dm

Interest in the electronic structure of InN has increased dramatically following improvements in its crystal growth and the subsequent revision of the accepted band gap from approximately 1.9 eV to the much lower value of approximately 0.64 eV.[1] The band gap of the $In_xGa_{1-x}N$ alloy system now spans the entire optical window from the near infrared to the UV.[2] Most experimental studies have focused on the optical properties of the band gap and there is a general paucity of spectroscopic measurements of the valence and conduction band densities of states in InN. Recently, the first combined x-ray photoemission spectroscopy (XPS) measurements and density functional theory (DFT) calculations of the valence band structure of single crystalline wurtzite InN have been reported.[3] Studies of well prepared polar InN samples using both high resolution angle resolved photoemission spectroscopy (ARPES) and high resolution electron energy-loss spectroscopy revealed significant electron accumulation near the film surface, leading to quantum well states in a layer extending from the surface up to 80Å below it.[4] Recent calculations have reported that the microscopic origin of the intrinsic electron accumulation at well-prepared polar InN surfaces is due to In-In bonds, within the In bilayer reconstruction, resulting in surface states above the conduction band minimum.[5] Surface states have yet to be observed on InN using ARPES, but In-adlayer reconstructions have been experimentally verified.[6]

We report here the results of a combined soft x-ray emission spectroscopy (XES) and soft x-ray absorption spectroscopy (XAS) study of the N 2*p partial* density of states (PDOS) of the valence and conduction bands. Theoretical calculations for the quasiparticle (QP) band structure were performed in the GW framework to calculate the N 2p PDOS. Good agreement between theory and experiment was obtained. Both XES and XAS involve a transition between electronic states within the solid, one of which is a localized core level (in this case the N *1s*). The measured emission or absorption spectrum can then be interpreted in terms of the density of occupied valence band or

unoccupied conduction band states, respectively.[7,8] Dipole selection rules ($\Delta l \pm 1$) govern the optical transition to or from the core-level,[7] and in the present case N *K*-edge XES and XAS measurements yield information on the N 2*p* PDOS. Unlike photoemission spectroscopy, these techniques are relatively insensitive to the quality of the sample surface and atomic cleaning is not necessary. This is especially beneficial for InN, where XPS studies have revealed how susceptible the surface is to In-droplet formation during cleaning cycles.[3] Furthermore, XES provides a direct measurement of the hybridization of shallow metal *d*-orbitals with ligand *p*-orbitals.[9] This is significant, since up to recently calculations of the electronic structure of InN relied on the experimental d-band binding energy and a careful consideration of the full effects of p-d repulsion.[3,10]

The 1 μm thick wurtzite InN($000\bar{1}$) thin films were grown on *c*-plane sapphire substrates by radio frequency plasma-assisted molecular beam epitaxy at 550˚C, at a rate of 0.9 μm/hour [11]. A low temperature (280˚C) thin InN buffer layer (approx. 30 nm) was grown between the InN film and the sapphire substrate. The samples were auto doped *n*-type with a measured carrier concentration of $n = 1\times10^{19}$ cm^{-3}. The N *K*-edge XAS and XES were measured at undulator beamline 7.0.1 at the Advanced Light Source (ALS), Lawrence Berkeley National Laboratory, which is equipped with a spherical grating monochromator. The absorption spectra were recorded in the total electron yield (TEY) and total florescent yield (TFY) modes with similar energy resolutions of 0.2 eV. For both measurements, the drain current of a mesh grid was used to monitor the incident light. The incident photon energy was calibrated to a cubic BN reference sample, measured during the experiments. Since the x-ray fluorescence process is weak compared to the competing non-radiative deexcitation channels,[12] a larger monochromator slit width is required to acquire reasonable counting statistics of ~30/sec. Emission spectra were recorded using a Nordgren-type grazing-incidence spherical grating spectrometer with an overall energy resolution of 0.56 eV at the N *K*-edge.[8] The emission energies

were calibrated to the emission spectrum of the N *K*-edge of the BN reference sample. Theoretical calculations of the PDOS for wurtzite InN were computed for comparison with the XES and XAS spectra. Since the final state in the x-ray emission process contains a hole in the valence band rather than the core-level, the soft x-ray emission spectra reflect the ground state PDOS provided that the final state rule is valid.[13] To first approximation, N *K*-edge XAS does reflect an image of the N 2*p*-orbital projected density of states. To first approximation, N K-edge XAS does reflect an image of the N 2p-orbital projected density of states. In general, XAS spectra should be compared to calculations which take into account core-hole effects, but these are neglected here. Each calculation was performed within the framework of hybrid DFT using the recently proposed HSE03 functional for exchange and correlation.[14] Beyond that, quasiparticle effects were taken into account by a subsequent GW correction of the HSE eigenvalues within the framework of Many Body Perturbation Theory. In the GW calculations, the Coulomb potential was screened fully dynamical using the RPA dielectric function based on the HSE eigenvalues and functions.[15] This approach to the QP band structure circumvents the problems related to the negative band gap of InN in DFT-LDA and was found to give reliable results for a large variety of semiconductors and insulators, especially those with shallow d-electrons.[16] The present approach goes beyond previously reported calculations since it is independent of the experimental *d*-band binding energy and provides access to the d-states DOS.[3] All calculations were performed using the Vienna Ab initio Simulation Package (VASP).[17] The calculated band gap was found to be 0.71 eV.

Figure 1 presents N *K*-edge XES ($2p \rightarrow 1s$) and XAS ($1s \rightarrow 2p$) spectra from InN on a common calibrated photon energy scale. The XES spectrum is recorded at normal emission using an incident excitation energy of 416.2 eV, well above the absorption threshold. The XAS spectra were recorded in both TFY and TEY modes with the photon beam incident at 20° to the sample normal. The XES

spectrum reflecting the N 2*p* PDOS is similar to that measured earlier from $In_xGa_{1-x}N$.[18] The valence band maximum (VBM) has been extrapolated from the leading edge of the emission peak, and was found to be at a photon energy of 394.56 eV. The TEY and TFY XAS spectra are quite similar to each other, with peaks at the same absorption energies. This similarity between the TFY and TEY spectra was also observed for XAS spectra measured at an incidence angle of 70˚ (not shown), and our results at 70˚ incidence agree with TFY XAS of InN reported earlier.[19-21] As will be discussed, the N *K*-edge absorption displays a strong dependence on the angle of incidence of the photon beam consistent with earlier TEY XAS measurements of group III nitrides (including InN). Furthermore, we observe a notable difference between the absorption edge onsets between the TFY and TEY modes for both angles of incidence. This is highlighted in the inset of Fig. 1, which displays an enlarged region close to the VBM. The TFY and TEY absorption onsets (determined from a straight line extrapolation of the leading edge of the absorption) are found to occur approximately 0.8 eV and 1.4 eV above the VBM, respectively. No angular difference in the respective absorption onsets was observed, which will be discussed later. TFY and TEY modes differ in being more bulk and surface sensitive, respectively.[22] The corresponding bulk Fermi (E_F) level for a carrier concentration of $n = 1\times10^{19}$ cm^{-3} is 0.86 eV above the VBM (for E_g = 0.64 eV, $m^*_0 = 0.042\ m_0$ with a non-parabolic conduction band and band gap shrinkage effects included). We note agreement between the separation of the extrapolated VBM and the onset of the absorption edge of the TFY XAS and the calculated bulk E_F to VBM separation. A larger separation is expected for the TEY XAS due to the Fermi level being pinned high above the CBM at the surface, due to the intrinsic electron accumulation. A value of 1.4 eV is in agreement with the E_F to VBM separation of InN from surface-sensitive XPS measurements.[3]

To compare the XES and XAS spectra with theoretical calculations, the spectra must be plotted on a common *binding* energy scale. This was achieved by rigidly shifting the emission and absorption spectra until the extrapolated experimental and calculated valence band maxima were in agreement. The XES spectra were also divided by E^3 (where E is the photon energy) to correct for the photon density of states' contribution to the transition rate.[23] Figure 2 a) presents the normalized XES/E^3 spectra for two incident photon energies: hν = 396.7 eV and 416.2 eV, corresponding to energies close to the absorption threshold and well above the threshold, respectively (see Fig. 1). The above-threshold XES spectral shape represents the local partial density of states (LPDOS), and has been plotted alongside the calculated N *2p* PDOS. For comparison, the theoretical N *2p* PDOS have been convoluted first using a Lorentzian with a full width at half maximum (FWHM) of 0.3 eV to account for lifetime broadening,[24] and were then further convoluted with a Gaussian of FWHM = 0.56 eV for account for experimental resolution. As is evident in Fig. 2, the spectral shape of the above-threshold XES and the calculated PDOS are in good agreement; in both cases a sharp low binding energy peak with a high binding energy shoulder is observed followed by a small well defined peak at ~ 5.5 eV below the VBM. We also note a weak peak at ~16 eV below the VBM in the N *K*-edge XES. This peak is due to transitions into the N 1*s* core-hole from electrons in N *2p* states hybridized with shallow core level In 4*d* electrons, and is shown magnified for the above-threshold XES spectrum Fig. 2a); the energy of the peak corresponds well with the calculated position of the In 4*d* - N 2*p* hybridized state. A clear shift in the peak closest the VBM towards higher photon energies (lower binding energies) is noted by changing the incident photon energy to 396.7 eV. The XES (hν = 396.7 eV) spectral shape consists of an incoherent LPDOS contribution and a **k**-selective coherent contribution.[25] In order to distinguish between these contributions, the largest LPDOS fraction (i.e the above-threshold XES spectrum) possible has been subtracted from the raw XES (hν

= 396.7 eV) spectrum whilst ensuring a non-negative difference (corresponding to the coherent contribution) - as described elsewhere[25] - and is displayed in Fig. 2 a). It was found that the highest emission energy peak corresponded to incident photon energy closest the absorption onset, consistent with the VBM of wurtzite InN lying at the zone center within the bulk. We note that an inverted valence band structure within the electron accumulation layer near the surface has recently been measured using ARPES.[26] This phenomena is difficult to observe with XES, since the XES sampling depth is much greater than the depth of the accumulation layer. Further work is required in order to determine **k**-resolved band structure of bulk InN with resonant XES, as recently attempted for GaN.[27] Due to its wurtzite structure, InN displays a strong angular dependence in N *K*-edge XAS spectra, as has been observed in all wurtzite group III nitrides.[20] The physical origin of this is due to the scalar multiplication in the matrix element of the absorption cross-section: for wurtzite crystals, if the polarization vector of the photon **E** is perpendicular to the **c** axis of the crystal (**E**$\perp$**c**) then transitions from the initial 1*s* state to the $2p_z$ states are forbidden. Likewise, under the **E**$\parallel$**c** condition transitions from the initial 1*s* state to the $2p_{xy}$ states are forbidden.[20,22] Figure 3 presents XAS spectra for two different incident angles: 70˚ and 20˚. These are recorded in TEY mode, but as noted above, the TFY spectra agree with the TEY spectra with respect to the main spectral features. Due to the geometry of the wurtzite crystal and the polarization of the synchrotron light, these spectra at 70˚ and 20˚ incidence correspond approximately to the **E**$\perp$**c** and **E**$\parallel$**c** conditions, respectively. The XAS spectrum recorded at an incidence angle of 20˚ is dominated by two peaks at approximately 8 and 10 eV above the VBM. If the angle of incidence is changed to 70˚, the intensity of the 8 eV feature increases dramatically, while that of the 10 eV peak is reduced. Figure 3 also presents the calculated N $2p_{xy}$ and N $2p_z$ contributions to the unoccupied PDOS. The theoretical spectra have been broadened for comparison with the measurements: first by convolution with a Lorentzian (FWHM = 0.3 eV)

followed by a Gaussian (FHWM = 0.2 eV) in order to account for lifetime broadening and the instrumental resolution. For both incident angles, we find good agreement between the XAS spectra and the corresponding PDOS. However, we do note a fixed 1eV shift between the experimental and theoretical features, which is attributed to excited-state self-energy corrections not included in the calculation and has been noted for comparisons between XAS and theory of GaN.[27] Furthermore, in agreement with previous TEY XAS experiments,[21] and our QP-corrected DFT calculated PDOS, the measured signal intensity was greater for the 70˚ spectra, corresponding to the dominant $2p_{xy}$ states for that geometry. However, once both spectra are scaled to the maximum peak intensity (as shown in figure 3), the extrapolated absorption edges are the same within error limits. This result is in contrast with earlier XAS results of InN that reported a 0.8 eV difference between the onsets.[21] Our results are in agreement with the calculated PDOS scaled in the same fashion.

In conclusion, we have presented an experimental and theoretical study of the valence and conduction band N *2p* density of states of wurtzite InN, using soft x-ray emission and absorption spectroscopies and *ab-initio* QP band structure calculations. We find excellent agreement between the spectra and the calculations, both in terms of the spectral shape and energetic location of peaks in the emission and absorption spectra, and the angular dependence of the absorption spectra.

This work was supported in part by the DOE under RF-06-PRD-001 (subcontract from University of Nevada, Las Vegas), and by the NSF under grant number DMR-0311792. The ALS is supported by the DOE, Materials Sciences Division under contract no. DE-AC03-76SF00098. Further support by the Deutsche Forschungsgemeinschaft under contract no. BE1346/18-2, and grants of computational time by the Leibnitz Rechenzentrum Munich is gratefully acknowledged.

Figure Captions:

Figure 1: InN XES and XAS spectra. The spectra are displayed on a calibrated photon energy axis. The VBM has been extrapolated from the leading edge of the XES to the baseline. The background corrected XAS spectra were recorded within the TEY (empty circles) and TFY (filled cicles) modes. The inset displays the enlarged region about the VBM. The onset of the absorption edges for the TFY and TEY are found to differ with respect to the VBM, in accordance with their respective bulk- and surface-sensitive natures. A larger separation between the VBM and absorption onset is noted for the TEY XAS, which is due to the Fermi level being pinned high above the CBM at the surface of InN. For the TFY XAS, the separation corresponds well to bulk Fermi level corresponding to its carrier concentration. The gray lines are guides to the eyes for the absorption onsets.

Figure 2: a) The normalized N *K*-edge XES spectra for two incident photon energies: hν = 396.7 eV (color online: red circles) and 416.2 eV (black circles) are displayed on a common binding energy axis referenced to the extrapolated VBM (= 0 eV). Also shown is the broadened theoretical QP-PDOS of the occupied N 2*p* orbitals. Agreement is observed between the energetic peaks of the calculated PDOS and above-threshold incoherent XES/E^3 (hν = 416.2 eV) spectrum. A In 4*d*-N 2*p* hybridized peak is noted in the magnified above-threshold XES/E^3 spectrum in

agreement with the calculated PDOS. Spectral shape differences are noted between the two emission spectra due to the lower incident energy emission having an additional **k**-selective coherent component.

b) The raw above-onset XES/E^3 ($h\nu$ = 396.7 eV) spectrum (color online: red) is plotted along with the incoherent local PDOS contribution (black line) and **k**-selective coherent contribution (gray filled area). See text for details.

Figure 3: Comparison of the background subtracted experimental N *K* -edge TEY absorption spectra (empty circles) at a) 20˚ and b) 70˚, and the corresponding weighted unoccupied theoretical PDOS (black line) vertically offset. A common binding energy axis has been used, and the effects of lifetime broadening and the instrumental broadening have been considered . A 3-point adjacent averaging smoothing (color online: thin red line) has been included to guide the eye.

References:

*Corresponding author. Electronic mail: lfjpiper@physics.org

1. J. Wu, W. Walukiewicz, K.M. Yu, J.W. Ager, E.E. Haller, H. Lu, W.J. Schaff, Y. Saito, and Y. Nanishi, Appl. Phys. Lett. **80**, 3967 (2002).

2. J. Wu, W. Walukiewicz, K.M. Yu, J.W. Ager, E.E. Haller, H. Lu, and W.J. Schaff, Appl. Phys. Lett. **80**, 4741 (2002).

3. L.F.J. Piper, T.D. Veal, P.H. Jefferson, C.F. McConville, F. Fuchs, J. Furthmuller, F. Bechstedt, H. Lu, and W.J. Schaff, Phys. Rev. B **72**, 245319 (2005).

4. I. Mahboob, T.D. Veal, C.F. McConville, H. Lu, and W.J. Schaff, Phys. Rev. Lett. **92**, 036804 (2004); L. Colakerol, T.D. Veal, H.K. Jeong, L. Plucinski, A. DeMasi, S. Wang, Y. Zhang, L.F.J. Piper, P.H. Jefferson, A. Fedorov, T.C. Chen, T.D. Moustakas, C.F. McConville, and K.E. Smith, Phys. Rev. Lett. **97**, 237601 (2006).

5. D. Segev and C.G. Van de Walle, Europhys. Lett. **76**, 305 (2006).

6. L.F.J. Piper, T.D. Veal, M. Walker, I. Mahboob, C.F. McConville, H. Lu, and W.J. Schaff, J Vac Sci Technol A **23**, 617 (2005); T.D. Veal, P.D.C. King, P.H. Jefferson, L.F.J. Piper, C.F. McConville, Lu. Hai, W.J. Schaff, P.A. Anderson, S.M. Durbin, D. Muto, H. Naoi, and Y. Nanishi, Phys. Rev. B ***(submitted)*** (2007).

7. A. Kotani and S. Shin, Rev. Mod. Phys. **73**, 203 (2001).

8. J. Nordgren, G. Bray, S. Cramm, R. Nyholm, J.E. Rubensson, and N. Wassdahl, Rev. Sci. Instrum. **60**, 1690 (1989).

9. C. McGuinness, C.B. Stagarescu, P.J. Ryan, J.E. Downes, D. Fu, and K.E. Smith, Phys. Rev. B **68**, 165104 (2003); P.-A. Glans, T. Learmonth, C. McGuinness, K.E. Smith, J. Guo, A. Walsh, G.W. Watson, and R.G. Egdell, Chem. Phys. Lett. **399**, 98 (2004); L.-C. Duda, C.B. Stagarescu, J. Downes, K.E. Smith, D. Korakakis, T.D. Moustakas, J. Guo, and J. Nordgren, Phys. Rev. B **58**, 1928 (1998).

10. F. Bechstedt and J. Furthmuller, J. Cryst. Growth **246**, 315 (2002).

11. T.P. Chen, C. Thomidis, J. Abell, W. Li, and T.D. Moustakas, J. Cryst. Growth **288**, 254 (2006).

12. M.O. Krause, J. Phys. Chem. Ref. Data **8**, 307 (1979).

13. U. von Barth and G. Grossmann, Phys. Rev. B **25**, 5150 (1982).

14. J. Heyd, G.E. Scuseria, and M. Ernzerhof, J. Chem. Phys. **118**, 8207 (2003).

15. M. Shishkin and G. Kresse, Phys. Rev. B **74**, 035101 (2006).

16. F. Fuchs, F. Furthmuller, F. Bechstedt, M. Shishkin, and G. Kresse, Phys. Rev. B ***(submitted)*** (2007).

17. G. Kresse and J. Furthmuller, Phys. Rev. B **54**, 11169 (1996).

18. P. Ryan, C. McGuinness, J.E. Downes, K.E. Smith, D. Doppalapudi, and T.D. Moustakas, Phys. Rev. B **65**, 205201 (2002).

19. W. Walukiewicz, J.W. Ager, K.M. Yu, Z. Liliental-Weber, J. Wu, S.X. Li, R.E. Jones, and J.D. Denlinger, J. Phys. D **39**, R83 (2006).

20. K. Lawniczak-Jablonska, T. Suski, I. Gorczyca, N.E. Christensen, K.E. Attenkofer, R.C.C. Perera, E.M. Gullikson, J.H. Underwood, D.L. Ederer, and Z.L. Weber, Phys. Rev. B **61**, 16623 (2000).

21. K. Lawniczak-Jablonska, T. Suski, Z. Liliental-Weber, E.M. Gullikson, J.H. Underwood, R.C.C. Perera, and T.J. Drummond, Appl. Phys. Lett. **70**, 2711 (1997).

22. J. Stöhr, **NEXAFS Spectroscopy** (Springer, Berlin, 1992).

23. W.L. O'Brien, J. Jia, Q.-Y. Dong, T.A. Callcott, D.R. Mueller, D.L. Ederer, and C.-C. Kao, Phys. Rev. B **47**, 15482 (1993).

24. C.B. Stagarescu, L.-C. Duda, K.E. Smith, J.H. Guo, J. Nordgren, R. Singh, and T.D. Moustakas, Phys. Rev. B **54**, 17335 (1996).

25. S. Eisebitt and W. Eberhardt, J. Elec. Spec. Related Phenom. **110-111**, 335 (2000).

26. L. Colakerol, S. Healy, E.P. O'Reilly, A. Fedorov, T.C. Chen, T.D. Moustakas, and K.E. Smith, Phys. Rev. Lett. ***(submitted)*** (2007).

27. V.N. Strocov, T. Schmitt, J.E. Rubensson, P. Blaha, T. Paskova, and P.O. Nilsson, Phys. Rev. B **72** (2005).

Figure 1. Piper et al., Electronic structure of InN studied using soft X-ray emission, soft X-ray absorption, and quasiparticle band structure calculations

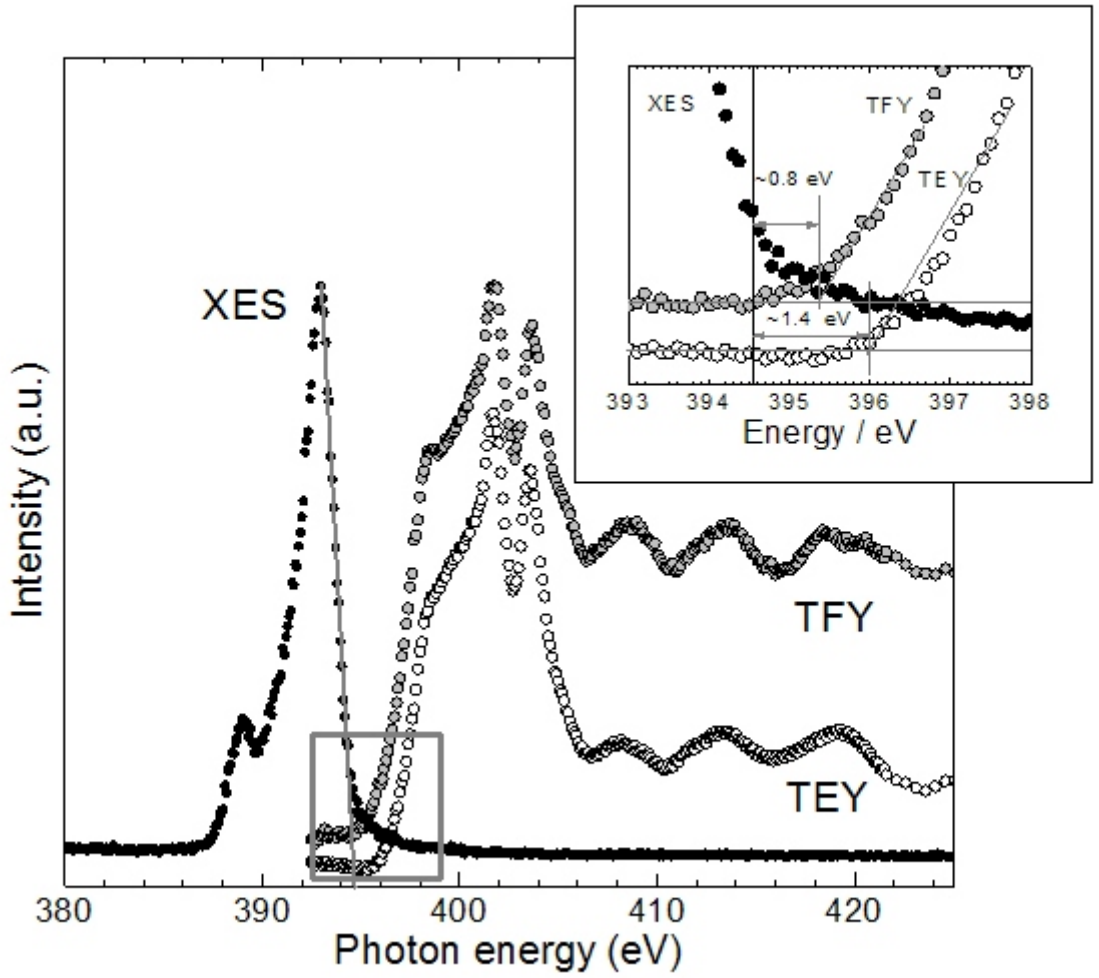

Figure 2. Piper et al., Electronic structure of InN studied using soft X-ray emission, soft X-ray absorption, and quasiparticle band structure calculations

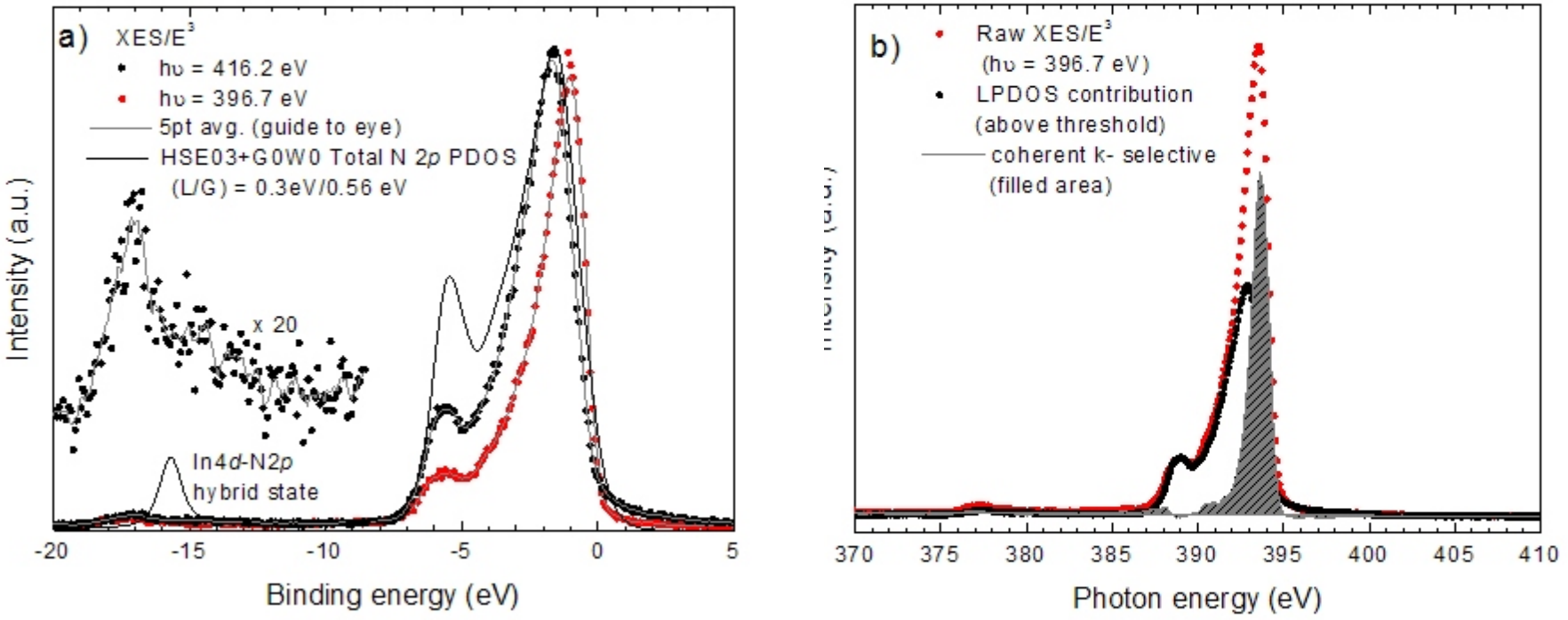

Figure 3. Piper et al., Electronic structure of InN studied using soft X-ray emission, soft X-ray absorption, and quasiparticle band structure calculations